AIAA JOURNAL
Vol. 48, No. 1, January 2010

Using Automatic Differentiation to Create a Nonlinear Reduced-Order-Model Aerodynamic Solver

Jeffrey P. Thomas,* Earl H. Dowell,† and Kenneth C. Hall‡
Duke University, Durham, North Carolina 27708–0300

DOI: 10.2514/1.36414

A novel nonlinear reduced-order-modeling technique for computational aerodynamics and aeroelasticity is presented. The method is based on a Taylor series expansion of a frequency-domain harmonic balance computational fluid dynamic solver residual. The first- and second-order gradient matrices and tensors of the Taylor series expansion are computed using automatic differentiation via FORTRAN 90/95 operator overloading. A Ritz-type expansion using proper orthogonal decomposition shapes is then used in the Taylor series expansion to create the nonlinear reduced-order model. The nonlinear reduced-order-modeling technique is applied to a viscous flow about an aeroelastic NLR 7301 airfoil model to determine limit cycle oscillations. Computational times are decreased from hours to seconds using the nonlinear reduced-order model.

Nomenclature

b, c	=	semichord and chord
$\bar{c}_{m_1}$	=	unsteady moment coefficient
$\bar{h}_0$, $\bar{\alpha}_0$	=	zeroth harmonic or mean airfoil plunge and pitch amplitude
$\bar{h}_1$, $\bar{\alpha}_1$	=	first harmonic unsteady airfoil plunge and pitch amplitude
M_∞	=	freestream Mach number
$\bar{p}_1$	=	unsteady pressure
Re, Im	=	real and imaginary parts
Re_∞	=	freestream Reynolds number
U_∞	=	freestream velocity
ω, $\bar{\omega}$	=	frequency and reduced frequency based on airfoil chord $\bar{\omega} = \omega c/U_\infty$

I. Introduction

COMPUTATIONAL fluid dynamic (CFD) models are becoming ever larger. Models with on the order of tens of millions of mesh points are now common. There is even talk of billion-point mesh models coming into existence in the near future. Although the ability to create and solve such large and dense mesh CFD models is of great benefit in modeling flows about complex geometric configurations, very long computational run times are typically required, and this makes the use of such models impractical for a great many engineering analysis and design problems.

In response to this challenge, in recent years, substantial research has been conducted in developing reduced-order models (ROMs) of high-dimensional CFD models with the goal of reducing computational times by orders of magnitude (see Dowell and Tang [1], Dowell and Hall [2], Lucia et al. [3], and Barone and Payne [4]). These ROMs are proving to be of great value, particularly for unsteady aerodynamic and aeroelastic analysis. CFD model systems, which can easily be on the order of millions of degrees of freedom (DOF), have been reduced to systems with as few as a dozen DOF while still retaining essentially the same accuracy as the full CFD model (see Willcox and Peraire [5], Thomas et al. [6,7], and Lieu and Farhat [8]).

Typically, these ROMs have been constructed for linearized time- or frequency-domain small-disturbance solvers that are dynamically linearized about some nonlinear stationary background flow state, which may include nonlinear steady flow features such as shocks and boundary layers. These ROMs are of great value for aeroelastic flutter onset analysis, for example, reducing the computational times by several orders of magnitude. Much of the work in recent years by the aeroelasticity group at Duke University has been directed toward the development of ROMs for linearized frequency-domain flow solvers.

The next major step in ROM development is to construct ROMs for dynamically nonlinear solvers for modeling those cases in which the amplitude of the unsteady flow oscillation is large and/or large changes occur in the mean background flow. Such ROMs are essential for matched-point flutter onset analysis as well as nonlinear limit cycle oscillation (LCO) analysis. These nonlinear ROMs will also be of great benefit for configuration design optimization for both steady and unsteady flows.

II. Objective

Our goal is the development of an accurate dynamically nonlinear ROM that will enable the rapid modeling of steady and unsteady aerodynamic flows and the associated fluid forces, particularly in the transonic Mach number region. Of particular interest is developing a method for rapidly determining the steady and unsteady aerodynamic forces created by large variations in steady flow parameters such as Mach number, angle of attack, and Reynolds number, as well as unsteady flow parameters such as unsteady frequency and unsteady plunge and/or pitch motion amplitudes or, more generally, changes in dynamic structural deformations. A complementary objective is to then couple the nonlinear ROM with a structural model for aeroelastic flutter, gust response, and LCO analysis.

III. Nonlinear ROM Methodology

Our approach is to construct a nonlinear ROM based on a Taylor series expansion of a given computational fluid dynamic solver residual in terms of the relevant model parameters. The method is similar in concept to the approach presented by Chen and White [9].

Presented as Paper 7115 at the 11th AIAA/ISSMO Multidisciplinary Analysis and Optimization Conference, Portsmouth, VA, 6–8 September 2006; received 31 December 2007; revision received 2 August 2009; accepted for publication 20 August 2009.

*Research Assistant Professor, Department of Mechanical Engineering and Materials Science. Senior Member AIAA.

†William Holland Hall Professor, Department of Mechanical Engineering and Materials Science, and Dean Emeritus, School of Engineering. Honorary Fellow AIAA.

‡Julian Francis Abele Professor, Department of Mechanical Engineering and Materials Science. Associate Fellow AIAA.

In the present case, we are using a nonlinear frequency-domain harmonic balance (HB) CFD solution method created at Duke University (Hall et al. [10] and Thomas et al. [11]). However, a time-domain CFD solver could be treated using a similar approach. A unique aspect of the method is that computational routines used to compute the matrices and tensors of the Taylor series expansion are created using automatic differentiation. Then a Ritz-type expansion using proper orthogonal decomposition shapes is used in conjunction with the Taylor series expansion to create the dynamically nonlinear reduced-order model. A special and very attractive feature of the method is that, in principle, it can be implemented within existing CFD solvers with minimal changes to the CFD solver code.

In recent years, the Duke University aeroelasticity research group has been active in the development of ROMs for linearized unsteady frequency-domain computational flow solvers [6,7,12]. These linearized unsteady frequency-domain computational flow solvers are capable of modeling unsteady aerodynamics as a result of infinitesimal structural motions for a fixed background steady flow condition. Although such methods are useful for aeroelastic flutter onset computations at fixed Mach numbers, they are not capable of treating large-amplitude structural motions or varying background flow conditions. In the following, we present a new technique for constructing a nonlinear ROM (NROM) about an existing computational fluid dynamic solver, which can then be used to model nonlinear unsteady aerodynamic effects brought about by changes in the mean background flow and finite amplitude structural motions. Results from the NROM are obtained at a much lower computational cost than directly using the nominal CFD solver. Such a NROM has the potential to be of great benefit for aerodynamic and aeroelastic sensitivity analysis and optimization. The concept for the Duke nonlinear reduced-order-modeling approach was first presented by Thomas et al. [13].

IV. HB Model Formulation

In the following, we consider a compressible CFD code, which uses a nonlinear frequency-domain harmonic balance solution procedure. The harmonic balance technique is implemented within the framework of a conventional time-domain CFD solver, and it provides an efficient method for modeling nonlinear unsteady aerodynamic effects brought about by finite amplitude structural motions of a prescribed frequency (see Hall et al. [10], Thomas et al. [11], and McMullen and Jameson [14] for further details).

The HB/CFD solver can be considered as a vector residual operator of the form

$$\mathbf{N}(\mathbf{Q}, \mathbf{L}) = \mathbf{0} \tag{1}$$

where $\mathbf{N}$ is the nonlinear vector residual operator of the HB/CFD method,

$$\mathbf{N} = \begin{Bmatrix} N_1 \\ N_2 \\ \vdots \\ N_{N_{\text{DOF}}} \end{Bmatrix} \tag{2}$$

and $\mathbf{Q}$ is the discrete HB/CFD solution:

$$\mathbf{Q} = \begin{Bmatrix} Q_1 \\ Q_2 \\ \vdots \\ Q_{N_{\text{DOF}}} \end{Bmatrix} \tag{3}$$

The number of degrees of freedom of the HB/CFD model, N_{DOF}, is the number of mesh points N_{mesh} times the number of equations being solved at each mesh point $N_{\text{Eqs.}}$ ($N_{\text{DOF}} = N_{\text{mesh}} \times N_{\text{Eqs.}}$). The vector $\mathbf{L}$ represents the HB/CFD flow solver input parameters:

$$\mathbf{L} = \begin{Bmatrix} M_\infty \\ Re_\infty \\ \bar{\alpha}_0 \\ \bar{\omega} \\ \bar{h}_1/b \\ \bar{\alpha}_1 \\ \vdots \end{Bmatrix} \tag{4}$$

V. Nonlinear ROM Formulation

First described by Thomas et al. [13], we again present the nonlinear ROM formulation for the sake of clarity. We first consider a specific vector of flow solver input parameters $\mathbf{L}_0$, and we call the solution associated with this set of HB/CFD solver input parameters $\mathbf{Q}_0$. $\mathbf{Q}_0$ as such satisfies

$$\mathbf{N}(\mathbf{Q}_0, \mathbf{L}_0) = \mathbf{0} \tag{5}$$

Next, we consider a slightly different set of input parameters, which we call $\mathbf{L}_1$. Our objective is to be able to rapidly compute the new HB/CFD flow solution $\mathbf{Q}_1$ corresponding to $\mathbf{L}_1$ using reduced-order modeling.

The concept behind the Duke NROM approach is to first do a Taylor series expansion for $\mathbf{N}(\mathbf{Q}_1, \mathbf{L}_1)$ about $\mathbf{N}(\mathbf{Q}_0, \mathbf{L}_0)$. For each element of $\mathbf{N}(\mathbf{Q}_1, \mathbf{L}_1)$, the Taylor series expansion can be expressed as

$$\begin{aligned} N_i(\mathbf{Q}_1, \mathbf{L}_1) = {} & N_i(\mathbf{Q}_0, \mathbf{L}_0) + \frac{\partial N_i}{\partial Q_j}\bigg|_{\mathbf{Q}_0,\mathbf{L}_0} \Delta Q_j + \frac{\partial N_i}{\partial L_j}\bigg|_{\mathbf{Q}_0,\mathbf{L}_0} \Delta L_j \\ & + \frac{1}{2}\frac{\partial^2 N_i}{\partial Q_j \partial Q_k}\bigg|_{\mathbf{Q}_0,\mathbf{L}_0} \Delta Q_j \Delta Q_k + \frac{1}{2}\frac{\partial^2 N_i}{\partial Q_j \partial L_k}\bigg|_{\mathbf{Q}_0,\mathbf{L}_0} \Delta Q_j \Delta L_k \\ & + \frac{1}{2}\frac{\partial^2 N_i}{\partial L_j \partial Q_k}\bigg|_{\mathbf{Q}_0,\mathbf{L}_0} \Delta L_j \Delta Q_k + \frac{1}{2}\frac{\partial^2 N_i}{\partial L_j \partial L_k}\bigg|_{\mathbf{Q}_0,\mathbf{L}_0} \Delta L_j \Delta L_k \\ & + \text{H.O.T.} = 0 \end{aligned} \tag{6}$$

where N_i is the ith element of the HB/CFD residual vector $\mathbf{N}$,

$$\Delta Q_j = Q_{j_1} - Q_{j_0} \tag{7}$$

$$\Delta L_j = L_{j_1} - L_{j_0} \tag{8}$$

and H.O.T. denotes third- and higher-order Taylor series expansion terms. We currently truncate the series to second-order; however, higher-order terms can be retained.

Next, we assume a Ritz-type expansion for $\Delta\mathbf{Q}$. That is, $\Delta\mathbf{Q}$ is expanded as

$$\Delta\mathbf{Q} = \mathbf{P}\Delta\mathbf{v} \tag{9}$$

where $\mathbf{P}$ is a $N_{\text{DOF}} \times N_v$ matrix consisting of N_v proper orthogonal decomposition (POD) mode shapes as column vectors. (See Hall et al. [12] and Thomas et al. [6] for further details on how POD mode shapes are created from flow solution snapshots.) This expansion can also be written as

$$\Delta Q_j = \frac{\partial P_j}{\partial v_m} v_m \tag{10}$$

We next let $\mathbf{r}$ be the vector defined by

$$\mathbf{r} = \mathbf{P}^T\mathbf{N} \tag{11}$$

Substituting the Ritz expansion equation (9) into Eq. (7) and premultiplying by $\mathbf{P}^T$ leads to the ROM form of the Taylor series expansion:

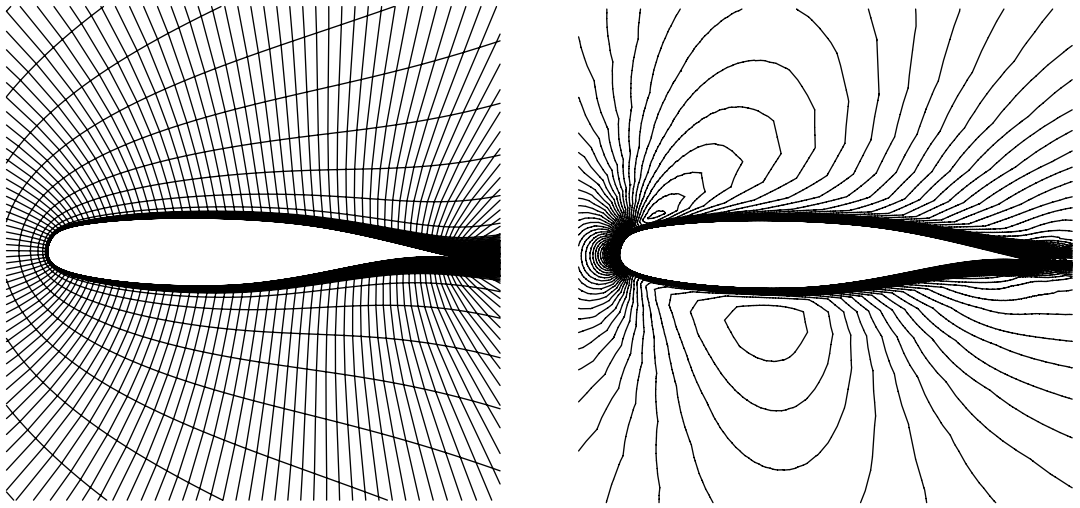

a) Computational grid b) Mach contours

Fig. 1 Computational grid and computed mach number contours for NLR 7301 airfoil section configuration; $M_\infty = 0.75$, $\bar{\alpha}_0 = 0.2°$, $Re_\infty = 1.727 \times 10^6$, $\bar{\omega} = 0.3$, and $\bar{\alpha}_1 = 3°$.

$$r_l(\mathbf{v}, \mathbf{L}_1) = \frac{\partial r_l}{\partial v_m}\bigg|_{\mathbf{Q}_0,\mathbf{L}_0} v_m + \frac{\partial r_l}{\partial L_j}\bigg|_{\mathbf{Q}_0,\mathbf{L}_0} \Delta L_j + \frac{1}{2}\frac{\partial^2 r_l}{\partial v_m \partial v_n}\bigg|_{\mathbf{Q}_0,\mathbf{L}_0} v_m v_n + \frac{1}{2}\frac{\partial^2 r_l}{\partial v_m \partial L_k}\bigg|_{\mathbf{Q}_0,\mathbf{L}_0} v_m \Delta L_k + \frac{1}{2}\frac{\partial^2 r_l}{\partial L_j \partial v_n}\bigg|_{\mathbf{Q}_0,\mathbf{L}_0} \Delta L_j v_n + \frac{1}{2}\frac{\partial^2 r_l}{\partial L_j \partial L_k}\bigg|_{\mathbf{Q}_0,\mathbf{L}_0} \Delta L_j \Delta L_k + \text{H.O.T.} = 0 \tag{12}$$

As noted previously, we truncate the system to second-order:

$$r_l(\mathbf{v}, \mathbf{L}_1) = \frac{\partial r_l}{\partial v_m}\bigg|_{\mathbf{Q}_0,\mathbf{L}_0} v_m + \frac{\partial r_l}{\partial L_j}\bigg|_{\mathbf{Q}_0,\mathbf{L}_0} \Delta L_j + \frac{1}{2}\frac{\partial^2 r_l}{\partial v_m \partial v_n}\bigg|_{\mathbf{Q}_0,\mathbf{L}_0} v_m v_n + \frac{1}{2}\frac{\partial^2 r_l}{\partial v_m \partial L_k}\bigg|_{\mathbf{Q}_0,\mathbf{L}_0} v_m \Delta L_k + \frac{1}{2}\frac{\partial^2 r_l}{\partial L_j \partial v_n}\bigg|_{\mathbf{Q}_0,\mathbf{L}_0} \Delta L_j v_n + \frac{1}{2}\frac{\partial^2 r_l}{\partial L_j \partial L_k}\bigg|_{\mathbf{Q}_0,\mathbf{L}_0} \Delta L_j \Delta L_k = 0 \tag{13}$$

Equation (13) is the NROM system, and we use the Newton–Raphson technique to solve for $\mathbf{v}$. We currently use FORTRAN 90/95 operator overloading to compute the Jacobians and tensors in Eq. (13). In Thomas et al. [13], we originally used an automatic differentiation tool known as TAPENADE [15] to derive the Jacobians and tensors in Eq. (13). We have recently switched to using FORTRAN 90/95 operator overloading (see, for example, Griewank [16]), and we like this approach a bit more since we are no longer dependent on a third-party external software tool to generate the gradient code. And furthermore, if we make any changes to our nominal CFD flow solver code, the resulting gradient Jacobians and tensors will reflect these changes. There is no need to generate new gradient code. Appendix A shows a simple example of how FORTRAN 90/95 operator overloading can be used to compute first- and second-order derivatives.

VI. NLR 7301 Airfoil Configuration

We first consider the application of the NROM technique to a transonic viscous flow about a real-world airfoil configuration. This airfoil configuration, the NLR 7301, has recently been studied experimentally for aeroelastic limit cycle oscillations (see Dietz et al. [17,18] and Schewe et al. [19]). Our research group has also recently conducted computational investigations of the nonlinear aeroelastic LCO response of this airfoil configuration (see Thomas et al. [20]). Our ultimate objective is to apply the NROM technique to our aeroelastic LCO solver to greatly reduce the computational time for computing nonlinear aeroelastic solutions.

For the NLR 7301 airfoil configuration, we consider a viscous transonic flow with a Mach number of $M_\infty = 0.75$, mean angle of attack of $\bar{\alpha}_0 = 0.2°$, and a Reynolds number of $Re_\infty = 1.727 \times 10^6$. For the unsteady portion of the flow, we consider pitching about the quarter-chord for a first harmonic unsteady pitch amplitude of $\bar{\alpha}_1 = 3°$ at a reduced frequency of $\bar{\omega} = 0.3$. The flow conditions correspond roughly to a LCO condition as predicted by Thomas et al. [20]. Thus, we consider a nominal flow $\mathbf{Q}_0$ based on a nominal set input parameters $\mathbf{L}_0$ given by

$$\mathbf{L}_0 = \begin{Bmatrix} M_\infty = 0.75 \\ \bar{\alpha}_0 = 0.2° \\ Re_\infty = 1.727 \times 10^6 \\ \bar{\omega} = 0.3 \\ \bar{h}_1/b = 0 \\ \bar{\alpha}_1 = 3° \end{Bmatrix} \tag{14}$$

Figure 1a shows the computational grid, and Fig. 1b shows computed mean flow Mach number contours for the NLR 7301 airfoil configuration for the $\mathbf{L}_0$ input parameter flow conditions. We next consider an alternate flow $\mathbf{Q}_1$ based on a set of input parameters $\mathbf{L}_1$ that are slightly different from the $\mathbf{L}_0$ flow solver input parameter conditions. Our objective is to compare first-order linear ROM results to second-order NROM results.

VII. NROM Results When Varying Multiple Independent Variables

We next consider a case in which we vary multiple HB/CFD flow solver independent variables. In this instance, we vary Mach number, mean angle of attack, unsteady reduced frequency, and unsteady pitch amplitude. We arbitrarily choose the input parameters $\mathbf{L}_1$ to be

$$\mathbf{L}_1 = \begin{Bmatrix} M_\infty = 0.79 \\ \bar{\alpha}_0 = 0.05° \\ Re_\infty = 1.727 \times 10^6 \\ \bar{\omega} = 0.225 \\ \bar{h}_1/b = 0 \\ \bar{\alpha}_1 = 3.75° \end{Bmatrix} \tag{15}$$

The changes in Mach number, mean angle of attack, unsteady reduced frequency, and unsteady pitch amplitude between the $\mathbf{L}_1$ and

$\mathbf{L}_0$ conditions correspond roughly to the same range of changes in flow solver input parameters for the LCO response calculations conducted by Thomas et al. [20]. These changes are large enough that nonlinear response of the HB/CFD solver is observed. Figure 2 shows the real (Fig. 2a) and imaginary (Fig. 2b) parts of the first harmonic unsteady surface pressure for both the $\mathbf{L}_0$ and $\mathbf{L}_1$ input parameter conditions. As can been seen, the solutions are considerably different.

We next compute a set of solution snapshots in order to create POD vectors. In this instance, we consider two solution snapshots for Mach numbers of $M_\infty = 0.77$ and 0.8. We then also consider two flow solution snapshots for mean angles of attack of $\bar{\alpha}_0 = 0.1$ and 0°, two flow solution snapshots for unsteady reduced frequencies of $\bar{\omega} = 0.25$ and 0.2, and two flow solution snapshots for unsteady pitch amplitudes of $\bar{\alpha}_1 = 3.5$ and 4°. This provides a total of eight snapshots from which we create eight POD mode shapes for use in the NROM. We have arbitrarily chosen the solution snapshots intervals. Our objective is to demonstrate that the second-order NROM is more accurate than the first-order ROM when using the same POD mode shapes.

Figure 3 shows the real (Fig. 3a) and imaginary (Fig. 3b) parts of the first harmonic unsteady surface pressure for the exact solution, along with first-order ROM and second-order NROM results, corresponding to the input parameters $\mathbf{L}_1$. As can be seen, the second-order NROM performs better than the first-order linear ROM, particularly for the imaginary part of the surface pressure.

VIII. NLR 7301 Aeroelastic Airfoil Configuration

One of the main objectives of developing the NROM technique is to provide an alternative to direct CFD computations for nonlinear unsteady aerodynamic modeling, which is a necessary ingredient for nonlinear aeroelastic limit cycle oscillation prediction. For demonstration purposes of the NROM methodology, we consider the NLR 7301 aeroelastic airfoil configuration of Dietz et al. [17,18] and Schewe et al. [19]. We also use the Newton–Raphson nonlinear frequency-domain aeroelastic solution technique presented by Thomas et al. [20].

Figure 4 shows LCO pitch amplitude $\bar{\alpha}_1$ versus reduced velocity V response trends for the NLR 7301 aeroelastic airfoil configuration. Shown are computed results for both inviscid and viscous models (from Thomas et al. [20]), in addition to an experimental result and two other computational studies. Clearly, viscous effects are important for predicting LCO. The goal is to use the NROM technique to model a portion of the viscous LCO response curve shown in Fig. 4.

As a first step, we consider using the NROM to model LCO about the full CFD model 3° pitch amplitude ($\bar{\alpha}_1 = 3°$) viscous-case data

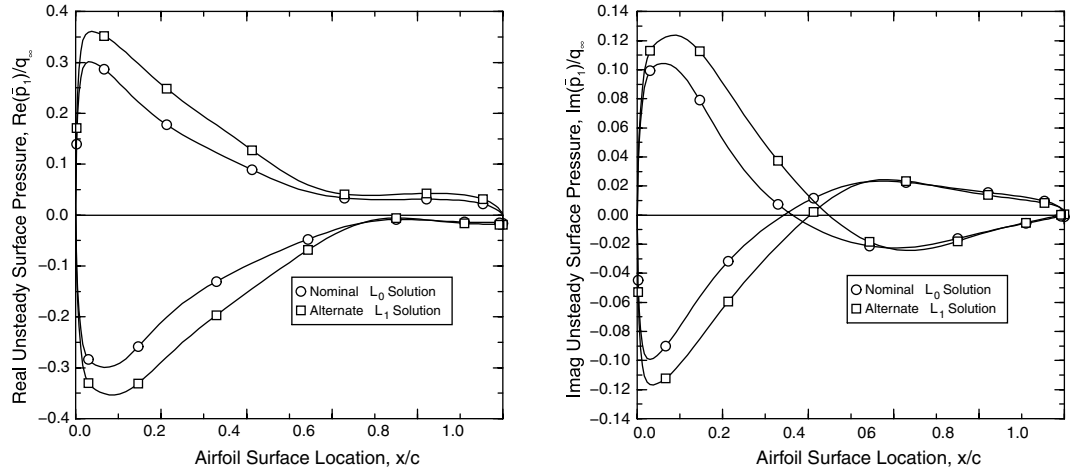

a) Real part b) Imaginary part

Fig. 2 Difference in unsteady surface pressure distributions between $\mathbf{L}_0$ and $\mathbf{L}_1$ HB/CFD flow solver input parameter cases.

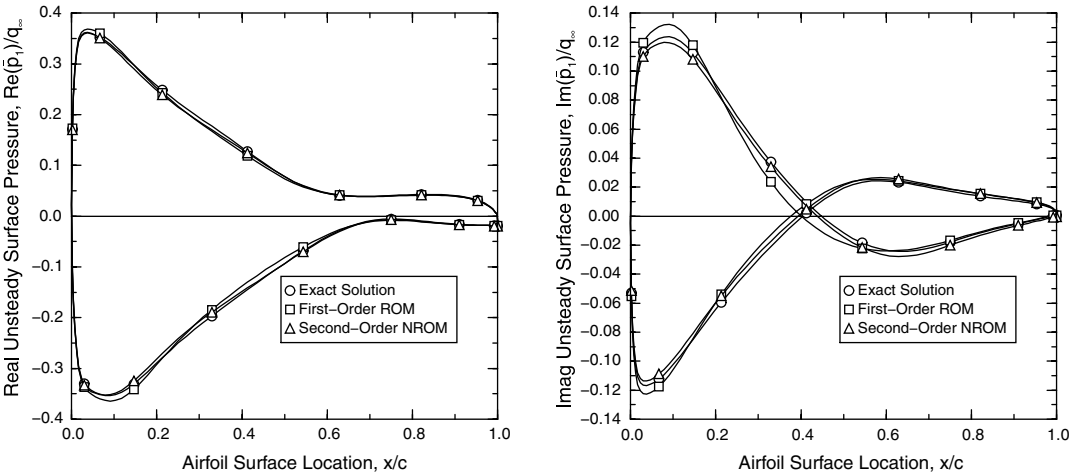

a) Real part b) Imaginary part

Fig. 3 Linear and nonlinear rom performance for real and imaginary unsteady pressure distributions; $M_\infty = 0.79$, $\bar{\alpha}_0 = 0.05°$, $Re_\infty = 1.727 \times 10^6$, $\bar{\omega} = 0.225$, and $\bar{\alpha}_1 = 3.75°$.

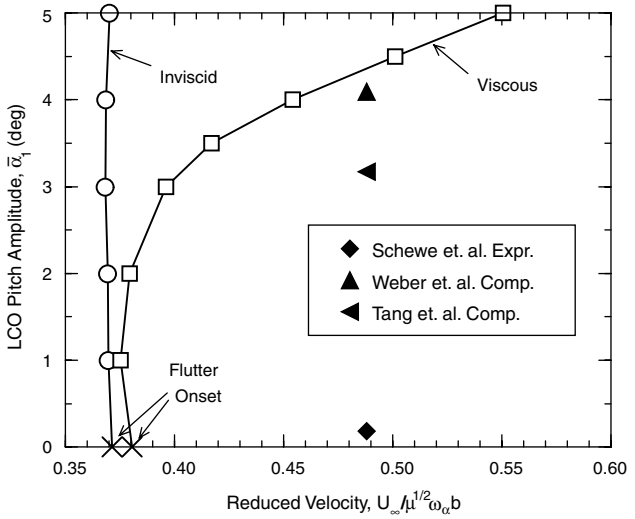

Fig. 4 LCO response trends for the NLR 7301 aeroelastic configuration.

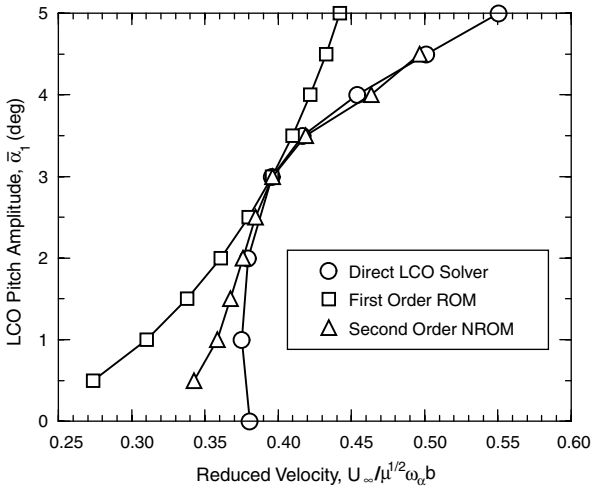

Fig. 5 LCO response trends for the NLR 7301 aeroelastic configuration including reduced-order-model results.

point. The computed aeroelastic LCO full HB/CFD model input parameter $\mathbf{L}$ conditions at the computed data point are

$$\mathbf{L} = \begin{Bmatrix} M_\infty = 0.75 \\ \bar{\alpha}_0 = 0.220451^\circ \\ \bar{\omega} = 0.293580 \\ \mathrm{Re}(\bar{h}_1/b) = 0.0595759 \\ \mathrm{Im}(\bar{h}_1/b) = 0.00630462 \\ \mathrm{Re}(\bar{\alpha}_1) = 3^\circ \\ \mathrm{Im}(\bar{\alpha}_1) = 0^\circ \end{Bmatrix} \tag{16}$$

We next consider the nominal flow $\mathbf{Q}_0$ as used for the NROM to be based on a nominal set of input parameters $\mathbf{L}_0$ given by

$$\mathbf{L}_0 = \begin{Bmatrix} M_\infty = 0.75 \\ \bar{\alpha}_0 = 0.2^\circ \\ \bar{\omega} = 0.29 \\ \mathrm{Re}(\bar{h}_1/b) = 0.06 \\ \mathrm{Im}(\bar{h}_1/b) = 0.006 \\ \mathrm{Re}(\bar{\alpha}_1) = 3^\circ \\ \mathrm{Im}(\bar{\alpha}_1) = 0^\circ \end{Bmatrix} \tag{17}$$

which are very close to the ($\bar{\alpha}_1 = 3^\circ$) LCO condition full HB/CFD model solution results.

Next, we compute solution snapshots for input parameters in the ranges of

$$\mathbf{L} = \begin{Bmatrix} M_\infty = 0.75 \\ \bar{\alpha}_0 = 0.2^\circ \pm 0.1^\circ \\ \bar{\omega} = 0.29 \pm 0.03 \\ \mathrm{Re}(\bar{h}_1/b) = 0.06 \pm 0.01 \\ \mathrm{Im}(\bar{h}_1/b) = 0.006 \pm 0.003 \\ \mathrm{Re}(\bar{\alpha}_1) = 0.5, 1.0, \ldots, 5.0^\circ \\ \mathrm{Im}(\bar{\alpha}_1) = 0^\circ \end{Bmatrix} \tag{18}$$

This leads to 17 snapshots from which we can construct 17 POD vectors for the NROM. In this case, the objective of this range of snapshots has been to enable the NROM to be able to model LCO in the range of a couple of degrees of unsteady pitch amplitude $\bar{\alpha}_1$ about the $\bar{\alpha}_1 = 3^\circ$ LCO condition.

Once the NROM has been constructed, it can be implemented within the aeroelastic solver. One simply substitutes calls normally made to the direct CFD solver with calls to the NROM.

Figure 5 shows computed LCO pitch amplitude $\bar{\alpha}_1$ versus reduced velocity V response trends using first-order linear ROM and second-order NROM models. As can be seen, the second-order NROM very well matches the full CFD model results about the $\bar{\alpha}_1 = 3^\circ$ LCO condition, even up to a LCO pitch amplitude of $\bar{\alpha}_1 = 4.5^\circ$. The computational expense of the NROM approach is only on the order of seconds as compared to the order of several hours, or even days, for the full HB/CFD model, for each data point in Fig. 5.

The major cost, however, for the nonlinear ROM (and linear ROM, likewise) is in computing the solution snapshots, which are necessary to construct the POD mode shapes. Each solution snapshot can take on the order of several thousand or even tens of thousands of iterations of the nominal HB/CFD solver.

To give the reader a sense of the computational cost of constructing the nonlinear ROM, let us say we can compute one CFD iteration per second. It usually takes on the order of 10,000 iterations to converge the residual of an unsteady harmonic balance CFD solution by six or more orders of magnitude, which is a level more than sufficient for solution convergence. So computing the 17 snapshots in the current example takes approximately 48 h (17 solutions times 10,000 iterations/solution times 1 s/iteration = 170,000 s, or approximately two days). Next, if we use all 17 POD vectors as computed from the 17 snapshots, then constructing the first-order Jacobians in Eq. (13) will take approximately 17 s, and constructing the second-order tensor terms in Eq. (13) will take about 17^2 s, or approximately 5 min. Computing the LCO curve by solving the resulting NROM then takes approximately 2–3 s for each data point.

IX. Conclusions

A method for creating a nonlinear reduced-order model of a computational fluid dynamic flow solver is presented. The technique is based on a Taylor series expansion of the flow solver residual together with a Ritz-type expansion using proper orthogonal decomposition shapes. Automatic differentiation is used to derive the Taylor series expansion of the fluid dynamic solver residual. Limit cycle oscillations for viscous flow about a NLR 7301 airfoil aeroelastic model have been determined with computational times for the reduced-order model on the order of seconds compared to hours for the full CFD model.

Appendix A: Sample FORTRAN 90/95 Operator Overloading Code for Computing Derivatives

Figure A1 is a simple example of FORTRAN 90/95 operator overloading code. In this example, we overload the multiplication operator (∗) to compute both first- and second-order gradients of a function. Division (/), addition (+), subtraction (−), power (∗∗), and intrinsic functions (sine, cosine, absolute value, etc.) can also be treated in a similar manner.

```
      module forward_module
      implicit none
!
!.... type definition containing variable and derivatives
      type d2_real
         real :: d0
         real :: d1
         real :: d2
      end type d2_real
!
!.... interface definitions
      interface operator (*)
         module procedure mult_op_22
      end interface
!
      contains
!
         function mult_op_22 (x,y) result (xy)
            type (d2_real), intent(in)  :: x
            type (d2_real), intent(in)  :: y
            type (d2_real)              :: xy
            xy.d0 = x.d0*y.d0
            xy.d1 = x.d1*y.d0 + x.d0*y.d1
            xy.d2 = x.d2*y.d0 + x.d0*y.d2 + x.d1*y.d1 + y.d1*x.d1
         end function mult_op_22
!
      end module forward_module
!
      program main
      use forward_module
      implicit none
!
      type(d2_real) :: f,x
!
      x%d0 = 3.
      x%d1 = 1.
!
      f = x*x
!
      write(*,*)
      write(*,*)'derivatives of f=x*x for x=3:'
      write(*,*)'----------------------------'
      write(*,*)'f(x=3)         = ',f%d0
      write(*,*)'df/dx(x=3)     = ',f%d1
      write(*,*)'d 2f/dx 2(x=3) = ',f%d2
      write(*,*)
!
      end program main
```

Fig. A1 Example of FORTRAN 90/95 operator overloading code.

When we run the example FORTRAN 90/95 operator overloading code, we obtain the following output:

```
derivatives of f=x*x for x=3:
----------------------------
f(x=3)         =    9.000000
df/dx(x=3)     =    6.000000
d 2f/dx 2(x=3) =    2.000000
```

which are the correct answers for

$$f(x=3) = x \times x = 3 \times 3 = 9$$

$$\frac{\mathrm{d}f}{\mathrm{d}x}(x=3) = 2 \times x = 2 \times 3 = 6$$

$$\frac{\mathrm{d}^2 f}{\mathrm{d}x^2}(x=3) = 2$$

For our nonlinear ROM code, we have written operator overloading code that can treat all the mathematical elements of the nominal harmonic balance flow solver code.

References

[1] Dowell, E. H., and Tang, D. M., *Dynamics of Very High Dimensional Systems*, World Scientific, Singapore, 2003.

[2] Dowell, E. H., and Hall, K. C., "Modeling of Fluid-Structure Interaction," *Annual Review of Fluid Mechanics*, Vol. 33, 2001, pp. 445–490. doi:10.1146/annurev.fluid.33.1.445

[3] Lucia, D. J., Beran, P. S., and Silva, W. A., "Reduced-Order Modeling: New Approaches for Computational Physics," *Progress in Aerospace Sciences*, Vol. 40, Nos. 1–2, Feb. 2004, pp. 51–117. doi:10.1016/j.paerosci.2003.12.001

[4] Barone, M. F., and Payne, J. L., "Methods for Simulation-Based Analysis of Fluid-Structure Interaction," Sandia National Labs., TR SAND2005-6573, Albuquerque, NM, 2005.

[5] Willcox, K., and Peraire, J., "Balanced Model Reduction Via the Proper Orthogonal Decomposition," *AIAA Journal*, Vol. 40, No. 11, Nov. 2002, pp. 2323–2330. doi:10.2514/2.1570

[6] Thomas, J. P., Dowell, E. H., and Hall, K. C., "Three-Dimensional Transonic Aeroelasticity Using Proper Orthogonal Decomposition-Based Reduced-Order Models," *Journal of Aircraft*, Vol. 40, No. 3, May–June 2003, pp. 544–551. doi:10.2514/2.3128

[7] Thomas, J. P., Dowell, E. H., and Hall, K. C., "Static/Dynamic Correction Approach for Reduced-Order Modeling of Unsteady Aerodynamics," *Journal of Aircraft*, Vol. 43, No. 4, July–Aug. 2006, pp. 865–878. doi:10.2514/1.12349

[8] Lieu, T., and Farhat, C., "Adaptation of POD-Based Aeroelastic ROMs for Varying Mach Number and Angle of Attack: Application to a Complete F-16 Configuration," AIAA Paper 2005-7666, 2005.

[9] Chen, Y., and White, J. K., "A Quadratic Method for Nonlinear Model Order Reduction," *2000 International Conference on Modeling and Simulation of Microsystems, Semiconductors, Sensors and Actuators*, Computational Publications, Cambridge, MA, 2000, pp. 477–480

[10] Hall, K. C., Thomas, J. P., and Clark, W. S., "Computation of Unsteady Nonlinear Flows in Cascades Using a Harmonic Balance Technique," *AIAA Journal*, Vol. 40, No. 5, 2002, pp. 879–886. doi:10.2514/2.1754

[11] Thomas, J. P., Dowell, E. H., and Hall, K. C., "Nonlinear Inviscid Aerodynamic Effects on Transonic Divergence, Flutter and Limit Cycle Oscillations," *AIAA Journal*, Vol. 40, No. 4, April 2002, pp. 638–646. doi:10.2514/2.1720

[12] Hall, K. C., Thomas, J. P., and Dowell, E. H., "Proper Orthogonal Decomposition Technique for Transonic Unsteady Aerodynamic Flows," *AIAA Journal*, Vol. 38, No. 10, Oct. 2000, pp. 1853–1862. doi:10.2514/2.867

[13] Thomas, J. P., Dowell, E. H., and Hall, K. C., "Using Automatic Differentiation to Create a Nonlinear Reduced Order Model of a Computational Fluid Dynamic Solver," 11th AIAA/ISSMO Multidisciplinary Analysis and Optimization Conference, Portsmouth, VA, AIAA Paper 2006-7115, 2006.

[14] McMullen, M. S., and Jameson, A., "The Computational Efficiency of Nonlinear Frequency Domain Methods," *Journal of Computational Physics*, Vol. 212, No. 2, March 2006, pp. 637–661. doi:10.1016/j.jcp.2005.07.021

[15] Hascoët, L., and Pascual, V., *TAPENADE 2.1 User's Guide*, Institut National de Recherche en Informatique et en Automatique, TR 0300, 2004, http://www.inria.fr/rrrt/rt-0300.html [retrieved 20 Oct. 2009].

[16] Griewank, A., *Evaluating Derivatives: Principles and Techniques of Algorithmic Differentiation*, Society for Industrial and Applied Mathematics, Philadelphia, 2000.

[17] Dietz, G., Schewe, G., and Mai, H., "Amplification and Amplitude Limitation of Heave/Pitch Limit-Cycle Oscillations Close to the Transonic Dip," *Journal of Fluids and Structures*, Vol. 22, No. 4, May 2006, pp. 505–527. doi:10.1016/j.jfluidstructs.2006.01.004

[18] Dietz, G., Schewe, G., and Mai, H., "Experiments on Heave/Pitch Limit-Cycle Oscillations of a Supercritical Airfoil Close to the Transonic Dip," *Journal of Fluids and Structures*, Vol. 19, No. 1, Jan. 2004, pp. 1–16. doi:10.1016/j.jfluidstructs.2003.07.019

[19] Schewe, G., Mai, H., and Dietz, G., "Nonlinear Effects in Transonic Flutter with Emphasis on Manifestations of Limit Cycle Oscillations," *Journal of Fluids and Structures*, Vol. 18, No. 1, Aug. 2003, pp. 3–22. doi:10.1016/S0889-9746(03)00085-9

[20] Thomas, J. P., Dowell, E. H., and Hall, K. C., "Modeling Viscous Transonic Limit Cycle Oscillation Behavior Using a Harmonic Balance Approach," *Journal of Aircraft*, Vol. 41, No. 6, Nov.–Dec. 2004, pp. 1266–1274. doi:10.2514/1.9839

P. Beran
Associate Editor